

24th DOE/NRC NUCLEAR AIR CLEANING AND TREATMENT CONFERENCE
DIFFUSIONAL ANALYSIS OF THE ADSORPTION OF METHYL IODIDE
ON SILVER EXCHANGED MORDENITE

R. T. Jubin
Chemical Technology Division
Oak Ridge National Laboratory
Oak Ridge, Tennessee 37831

and

R. M. Counce
Department of Chemical Engineering
University of Tennessee
Knoxville, Tennessee 37916

Abstract

The removal of organic iodides from off-gas streams is an important step in controlling the release of radioactive iodine to the environment during the treatment of radioactive wastes or the processing of some irradiated materials. Nine-well accepted mass transfer models were evaluated for their ability to adequately explain the observed CH_3I uptake behavior onto the Ag°Z . Linear and multidimensional regression techniques were used to estimate the diffusion constants and other model parameters, which then permitted the selection of an appropriate mass transfer model.

Although a number of studies have been conducted to evaluate the loading of both elemental and methyl iodide on silver-exchanged mordenite, these studies focused primarily on the macro scale (deep bed) while evaluating the material under a broad range of process conditions and contaminants for total bed loading at the time of breakthrough. A few studies evaluated equilibrium or maximum loading. Thus, to date, only bulk loading data exist for the adsorption of CH_3I onto Ag°Z . Hence this is believed to be the first study to quantify the controlling mass transfer mechanisms of this process.

It can be concluded from the analysis of the experimental data obtained by the "single-pellet" -type experiments and for the process conditions used in this study that the overall mass transfer rate associated with the adsorption of CH_3I onto Ag°Z is affected by both micropore and macropore diffusion. The macropore diffusion rate was significantly faster than the micropore diffusion, resulting in a two-step adsorption behavior which was adequately modeled by a bimodal pore distribution model. The micropore diffusivity was determined to be on the order of $2 \times 10^{-14} \text{ cm}^2/\text{s}$. The system was also shown to be isothermal under all conditions of this study.

Introduction

One of the promising solid sorbent technologies for the removal and retention of iodine in terms of performance and simplicity is the adsorption on hydrogen-reduced silver mordenite (Ag°Z). This form of the sorbent has been reported by several researchers [Thomas et al. (1977), Jubin (1980, 1982), Scheele et al. (1983), and Sheele and Burger (1987)] to be more effective in trapping I_2 and CH_3I than the ionic silver mordenite (AgZ). Although a number of studies have been conducted to evaluate the loading of both elemental and methyl iodide on silver-exchanged mordenite, they focused primarily on the macro scale (deep bed) while evaluating the material under a broad range of process conditions and

24th DOE/NRC NUCLEAR AIR CLEANING AND TREATMENT CONFERENCE

contaminants for total bed loading at the time of breakthrough. Thus for the most part, only bulk loading data appear to exist in the literature for the adsorption of CH_3I onto AgZ or Ag°Z . The specific objective was to provide sufficient insight into the adsorption process to allow the determination of the primary controlling mechanisms and diffusion and/or reaction coefficients associated with the process.

Theory and Assumptions

The process of physical adsorption in porous adsorbent material is generally extremely rapid according to Kärger and Ruthven (1992). As a result, in most cases, mass or heat transfer resistances are the controlling factors for the overall rate of adsorption. Kärger and Ruthven (1992) provided an outstanding discussion on the diffusional resistances in zeolite pellets. What follows is a summary of that discussion as it applies to the problem at hand.

According to the International Union of Pure and Applied Chemistry (IUPAC) classification, pores with a diameter less than 20 Å are considered micropores while pores with a diameter greater than 500 Å are classified as macropores. The region between 20 and 500 Å is classified as mesopores (Kärger and Ruthven, 1992). The mass transport in each of these three size regions is controlled by different diffusion mechanisms. In the macropores, interactions between the pore walls and the diffusing molecule are minor and generally bulk diffusion is observed. Typically, the macropore provides only limited adsorption capacity but may significantly impact the mass transfer rates. As the size of the pore decreases, the interactions with the walls become increasingly important. In the mesopore region, diffusion control is generally associated with Knudsen diffusion; however, both surface diffusion and capillary effects may play significant roles. In the micropore region, surface forces are the most significant, as the diffusing molecule interacts with the wall more frequently than with other diffusing molecules. This form of diffusion is also known as "intracrystalline" diffusion. Micropore diffusion is also quite different from the diffusion processes in either the macropore or mesopore regions in that it is an activated process. This implies that the observed diffusion rate, if this mechanism could be isolated, would vary with temperature in accordance with an Arrhenius form equation:

$$D_c = D_\infty e^{-E_a/RT} \quad (1)$$

Kärger and Ruthven (1992) further indicate that the analysis of loading data obtained for zeolite crystals that are "sufficiently large" can generally be accomplished through the use of the simple single micropore diffusion resistance model. However, in the case of commercial pelleted adsorbents, there is often a continuous range of pore sizes, which includes micropores, mesopores, and macropores. The analysis of many commercially available zeolite adsorbents is a bit more tractable because these materials are formed from small microporous particles of the actual zeolite crystal to produce a macroporous pellet of a manageable size. In such pellets, the pore size distribution is reported to often exhibit a bimodal-type distribution. In this situation, it is possible that the mass transport is controlled by macropore and/or micropore diffusion resistances.

General Assumptions and Simplifications

In most cases, modeling of the diffusion processes in porous media requires some type of simplifying assumptions. These generally involve the definition of structure of the adsorbent material, the nature or order of the chemical reactions and thermal effects associated with the heat of reaction and adsorption, and finally the behavior of the diffusion coefficient.

24th DOE/NRC NUCLEAR AIR CLEANING AND TREATMENT CONFERENCE

Commercially available extruded adsorbents are not of uniform size. While the diameter appears to be nearly the same, the length varies greatly. It is generally accepted to use an equivalent spherical radius, \bar{r} , defined as the radius of a sphere having the same external surface-to-volume ratio. In the analysis of Kärger and Ruthven (1992), this is shown to be valid for small changes in conversion. In the case of an infinite cylinder and a material with the equivalent spherical radius determined as stated above, the dimensionless time required to reach 90% conversion is different by about 25%. At 50% conversion, the error is <5%.

The second assumption deals with the structure of the pellet itself, as this will in large part define the nature of the model. The structure of the solid pellet has been conceptualized in numerous ways (Ramachandran and Doraiswamy, 1982; and Kulkarni and Doraiswamy, 1986), ranging from the simplest approach of a spherical, homogenous, nonporous pellet to a porous pellet containing subparticles that may also be porous (Kärger and Ruthven, 1992). The introduction of some type of pore structure also requires an assumption concerning the pore behavior. The pore can either remain constant or change as a function of time.

A third assumption that must be validated is that the process can be considered to occur under isothermal conditions. The models described below assume that the system being studied is isothermal. However, when studying an adsorption/reaction process, the possibility that this assumptions might be invalid as a result of the heat effects from adsorption and/or reaction must be considered. In such a case, the heat effects, which may be significant, must be accounted for in the analysis used to examine the experimental data. The assumption of isothermal conditions is generally only valid when the sorption rates are relatively slow (Kärger and Ruthven, 1992).

Lee and Ruthven (1978) describe the three possible resistances to heat transfer. These are (1) the resistance to heat transfer from the external surface of the pellet to the surrounding fluid; (2) the resistance to heat transfer from the external surface of an individual particle within the pellet or, in other words, the internal heat transfer resistances; or (3) the resistance to heat conduction within the individual particle. It was shown that for all cases the heat transfer from the external surface will be slower than heat transfer between the crystals of the sample. Based on this analysis, the temperature throughout the sample was uniform.

To determine the significance of the potential nonisothermal behavior, an analysis of maximum temperature variation due to the heat of adsorption and chemical reaction was made. The analysis of this system by Jubin (1995), using conservative assumptions for all variables, indicated a maximum delta temperature between the pellet and the bulk fluid as a result of both the heat of adsorption and chemical reaction of 0.37°C. Based on this result, it clearly appeared that the assumption of isothermal adsorption was substantiated.

Finally assumptions about the stability of the process system used in the experimental determinations are generally made. One of the common process assumptions is that of constant bulk gas-phase composition. This is either based on the use of a very large system, a true constant pressure system, or by careful control of a flowing gas stream. If this assumption is not made, then the changing composition of the gas phase must be addressed in the model.

Shrinking or Unreacted Core Model

One of the classic models used to describe noncatalytic reactions of solid particles with a surrounding fluid is the shrinking or unreacted core model. This model, as described by Levenspiel (1972, 1979), was developed by Yagi and Kunii in 1955 and contains five sequential steps for the gaseous reactant and product components.

24th DOE/NRC NUCLEAR AIR CLEANING AND TREATMENT CONFERENCE

For the reactant gases:

1. Diffusion through a boundary layer gas film which surrounds the solid particle.
2. Diffusion through the particle to the surface of the unreacted core.
3. Reaction with the solid reactant at the surface of the solid core.

And for the product gases:

4. Diffusion back through the reacted portion of the particle to the outside surface of the particle.
5. Diffusion through the boundary layer gas film surrounding the solid particle.

It was noted by Levenspiel (1972) that there may be significant variations in the relative importance of these five steps, depending on the relative magnitude of the associated resistances to mass transfer. Furthermore, in some situations, some of these steps are not relevant. For example, in the case of an irreversible reaction, steps 4 and 5 do not contribute directly to the observed resistances to the reactions. The same is true of a reaction producing no gaseous products.

The basic conversion equations for the first three steps have been developed. For a gas-solid reaction of the general form



and constant-size spherical particles, the following conversion-time expressions are relevant for the first three resistances and can be used to compare the observed loading rate data with the theoretical uptake curve.

Individual Controlling Resistances

In terms of the flux, the equations describing film diffusion control can be written based on either the moles of the diffusing component, A , or the moles of the solid reactant, B , that is reacted with A according to Eq. (2):

$$-\frac{1}{S_{ex}} \frac{dN_B}{dt} = -\frac{1}{4\pi r_a^2} \frac{dN_B}{dt} = -\frac{b}{4\pi r_a^2} \frac{dN_A}{dt} = bk_g (C_{Ag} - C_{As}) \quad (3)$$

For the limiting case when there is only film diffusion control, C_{As} approaches 0. And the fractional conversion, X_B , can be expressed in terms of the unreacted core radius by

$$\frac{t}{\tau_{gasfilm}} = 1 - \left(\frac{r_c}{r_a} \right)^3 = X_B, \quad (4)$$

where the time for total conversion is given by

$$\tau_{gasfilm} = \frac{\rho_B r_a}{3bk_g C_{Ag}} \quad (5)$$

In a similar manner, expressions can be written for the case of ash diffusion alone. The resulting expression in terms of fractional conversion is

$$\frac{t}{\tau_{ash}} = 1 - 3(1 - X_B)^{2/3} + 2(1 - X_B), \quad (6)$$

where the time to complete conversion is given by

$$\tau_{ash} = \frac{\rho_B r_a^2}{6bD_e C_{Ag}}. \quad (7)$$

For chemical reaction control (rxn), the relationship for the conversion vs time is given by

$$\frac{t}{\tau_{rxn}} = 1 - \frac{r_c}{r_a} = 1 - (1 - X_B)^{1/3}, \quad (8)$$

where k_s is the assumed first-order reaction constant. The time to complete conversion is given by

$$\tau_{rxn} = \frac{\rho_B r_a}{bk_s C_{Ag}}. \quad (9)$$

Full Shrinking Core Model

In many situations, more than one of these resistances is a factor in determining the observed rate of conversion of the particle. The three individual rate expressions can be combined into a single expression (Levenspiel 1972, 1979).

$$-\frac{1}{S_{ex}} \frac{dN_B}{dt} = \left[\frac{b}{\frac{1}{k_g} + \frac{r_a(r_a - r_c)}{r_c D_e} + \frac{r_a^2}{r_c^2 k_s}} \right] C_{Ag}. \quad (10)$$

This expression can easily be converted into a more usable form for the analysis of the gravimetric loading data by expressing the unreacted core radius, r_c , in terms of conversion, found in Eq. (4), yielding

$$-\frac{1}{S_{ex}} \frac{dN_A}{dt} = \left[\frac{b}{\frac{1}{k_g} + \frac{r_a(1 - (1 - X_B)^{1/3})}{(1 - X_B)^{1/3} D_e} + \frac{1}{(1 - X_B)^{2/3} k_s}} \right] C_{Ag}. \quad (11)$$

This is then an expression that can be used to determine the values of the three adjustable parameters through a process of curve fitting to minimize the error between experimentally obtained flux or loading data and the calculated values.

24th DOE/NRC NUCLEAR AIR CLEANING AND TREATMENT CONFERENCE

Alternately, it has been shown by Levenspiel (1972, 1979) that the total time to reach a given conversion is the sum of the times for the individual mechanisms to reach the same conversion. In other words,

$$t_{total} = t_{gasfilm} + t_{ash} + t_{rxn}. \quad (12)$$

Likewise, for the complete conversion, the time is given by

$$\tau_{total} = \tau_{gasfilm} + \tau_{ash} + \tau_{rxn}. \quad (13)$$

By replacing the expressions for the individual times to reach a set conversion given by Eqs. (4), (6), and (8) for the individual times into Eq. (12), an expression is obtained that allows the determination of the extent of the conversion for any value of time. It should be noted that the conversion is found as the root of the following equation:

$$t_{total} = X_B \tau_{gasfilm} + \left[1 - 3(1 - X_B)^{2/3} + 2(1 - X_B) \right] \tau_{ash} + \left[1 - (1 - X_B)^{1/3} \right] \tau_{rxn}. \quad (14)$$

Isothermal Models for Porous Media

The previous models do not consider the nature of the media, which in the case of zeolites may be important. Kärger and Ruthven (1992) summarize numerous studies which have focused on the adsorption from the gas phase into a porous zeolite-type structure. In general terms, these studies attempted to incorporate the porous nature of the zeolite pellets by addressing diffusional resistances arising from (1) the micropores, (2) the macropores, or (3) a combination of both macropore and micropore resistance. These models are further summarized as follows.

Micropore Diffusion Controlling

For the case of micropore diffusion alone, the following transient sorption expression is presented by Kärger and Ruthven (1992):

$$X_B = \frac{m_t}{m_\infty} = 1 - \frac{6}{\pi^2} \sum_{n=1}^{\infty} \frac{1}{n^2} \exp\left(-\frac{n^2 \pi^2 D_c t}{r_i^2}\right). \quad (15)$$

The two primary assumptions that must be noted are the use of constant diffusivity and that the change in the adsorbed phase concentration is small such that gas phase or surface composition remains constant (Ruthven, 1984).

This model reduces to

$$X_B = \frac{m_t}{m_\infty} = 1 - \frac{6}{\pi^2} \exp\left(-\frac{\pi^2 D_c t}{r_i^2}\right) \quad (16)$$

as the time term becomes large. Kärger and Ruthven (1992) point out that a plot of $\ln[1 - m_t/m_\infty]$ vs t should approach a straight line. This line will have a slope of $-\pi^2 D_c / r_i^2$ and an intercept of $\ln(6/\pi^2)$.

Macropore Diffusion Controlling

For macropore diffusion the solution is the same with the D_c/r_i^2 term replaced by

$$\frac{D_p}{r_a^2} \left(\frac{1}{1 + K^*(1 - \epsilon_p) / \epsilon_p} \right), \quad (17)$$

where K^* is an equilibrium constant which has an Arrhenius-type temperature dependence.

Combined Micropore and Macropore Diffusion Control

Dual-resistance systems in biporous media have been studied by several researchers. Ruckenstein et al. (1971), discussing the dissertation of Vaidyanathan (1971), pointed out that the macropore diffusivity and micropore diffusivity may, in many cases, be quite different by orders of magnitude. In such a case, the observed diffusion process may be significantly affected by the particular structure of the porous solid. The model developed by Vaidyanathan (1971) appears to be the first to address the analysis of transient sorption with the competing effects of macropore diffusion and micropore diffusion combined. The assumptions made in the development of this model are as follows:

1. The system is isothermal.
2. The particle is spherical and composed of small uniform spherical microporous particles.
3. The sorbent is exposed to an infinite source of sorbate such that the surface concentration is constant.
4. The sorbent is exposed to a step change in sorbate concentration at time zero.
5. Adsorption occurs at the walls of both the macropores and the micropores.
6. Linear isotherms apply.

Ma and Lee (1976) and Lee (1978) extended the original model to address the case of a finite quantity of sorbate. Of these, the model proposed by Lee appeared to be a bit simpler and faster in terms of computer time to apply as it contained only one double summation and the others contained the ratio of two double summations. In the case of constant gas-phase concentrations, the mathematical solution developed by Lee simplifies to

$$X_B = \frac{m_t}{m_\infty} = 1 - \frac{18}{\beta + 3\alpha} \sum_{m=1}^{\infty} \sum_{n=1}^{\infty} \left(\frac{n^2 \pi^2}{p_{n,m}^4} \right) \frac{e^{-p_{n,m}^2 D_c t / r_i^2}}{\left\{ \alpha + \frac{\beta}{2} \left[1 + \frac{\cot(p_{n,m})}{p_{n,m}} (p_{n,m} \cot(p_{n,m}) - 1) \right] \right\}}, \quad (18)$$

where

$$\alpha = \frac{D_c r_a^2}{r_i^2 D_p}, \quad (19)$$

$$\beta = \frac{3\alpha(1 - \epsilon_p)q_\infty}{\epsilon_p C_{A,0}}, \text{ and} \quad (20)$$

$p_{n,m}$ is given by the roots of the transcendental equation

$$\alpha p_{n,m}^2 - n^2 \pi^2 = \beta (p_{n,m} \cot(p_{n,m}) - 1) \quad (21)$$

Vaidyanathan (1971) discussed the physical significance of the α and β terms. α is the ratio of the time constants for macropore-to-micropore diffusion. For values of α less than 10^{-3} , macropore diffusion is much faster than micropore diffusion and the process can be considered to be a two-step process for all practical purposes. For values of α greater than 10^{+2} , macropore diffusion controls (Ruckenstein et al., 1971). In the range of α between these two limiting cases, both mechanisms are important. The term $\beta/3\alpha$ represents the ratio of sorption in the micropores to macropores at equilibrium. Thus a large value would indicate sorption primarily in the micropores.

Detailed description of other models that were evaluated for potential application to understand the behavior observed for this system may be found in Jubin (1995). These models include

- progressive conversion or volume reaction,
- nonisothermal micropore/macropore diffusion, and
- nonisothermal bed diffusion controlling.

Experimental Objectives

Conditions

As in numerous other studies [Jubin (1980, 1982), Burger and Scheele (1981), Scheele et al. (1983), and Scheele and Burger (1987)], methyl iodide was chosen as the chemical form for the iodine in this study because it is a more difficult form to retain in an adsorption process than elemental iodine. If CH_3I can be successfully retained on the silver mordenite, then the elemental iodine will also be retained (Scheele and Burger, 1987).

Experimental data were collected over a range of conditions selected to differentiate between the anticipated primary controlling mechanisms, and further data were collected to evaluate specific process behavior observed in the initial series of tests. The variables considered were (1) pellet diameter, (2) methyl iodide concentration, (3) gas velocity, (4) temperature, and, later in the study, (5) water vapor content of the carrier gas. The first four conditions were selected to examine the effects of these primary variables by varying each one while holding the others at a standard condition. Two duplicate tests were planned to allow a determination of the level of experimental error. Table 1 provides a listing of the ranges considered for each of the independent variables.

Following the completion of the initial series of tests, T3 to T13, 13 additional tests were conducted to explore specific aspects of this process and to gain further clarification on the behavior observed during the initial tests. Four specific avenues examined (1) the effects of either increasing or decreasing the water vapor content of the air, (2) further lowering of the gas velocity, (3) lower CH_3I concentration, and (4) lower operating temperatures. Two unique runs were also conducted, the first to determine the amount of water adsorbed from the instrument air and the second to determine the CH_3I loading on the zeolite media without chemical reaction occurring. Table 2 presents a listing of the conditions studied in each test.

Table 1 General test conditions.

Variable	Range or values considered
Pellet diameter (in.)	1/16 and 1/8
Gas velocity (m/min)	1, 2, 5, and 10
Methyl iodide concentration (mg/m ³)	250, 500, 1000 , and 1500
Temperature (°C)	125, 150 , and 200
Water content [dew point (°C)]	-40, -15 to -18 , -11

Note: Bold values were considered reference conditions.

Following the completion of the initial series of tests, T3 to T13, 13 additional tests were conducted to explore specific aspects of this process and to gain further clarification on the behavior observed during the initial tests. Four specific avenues examined (1) the effects of either increasing or decreasing the water vapor content of the air, (2) further lowering of the gas velocity, (3) lower CH₃I concentration, and (4) lower operating temperatures. Two unique runs were also conducted, the first to determine the amount of water adsorbed from the instrument air and the second to determine the CH₃I loading on the zeolite media without chemical reaction occurring. Table 2 presents a listing of the conditions studied in each test.

These supplemental tests specifically provided data on the impact of lower gas velocities (T15, T16, and T18) in an effort to resolve any effects of the gas film and lower CH₃I concentrations (T14) on possible reaction rate controlling conditions. The impacts of variations in the water vapor content of the gas stream were examined by adding a small additional amount of water vapor (T13) and by further drying the instrument air carrier gas (T18).

Test Equipment

Figure 1 is a schematic diagram of the process system showing the principal equipment components. The entire system was located inside a walk-in laboratory hood, with the exception of the dry air, hydrogen/argon and nitrogen cylinders, and the process control and data collection instrumentation.

To briefly describe the test system, a stream of dilute methyl iodide was fed into the test reaction chamber in which the bed containing the known quantity of selected sorbent material was located. The test bed, composed of a thin layer of Ag^oZ pellets, one to two pellets deep, was supported by a stainless steel wire basket, which was lowered into a glass gas reaction chamber. In this system, a thin layer of adsorbent media was exposed to the sorbate stream such that all pellets were exposed to a uniform gas composition. Thus the effects of a changing gas composition through the test bed were considered to be negligible. This method was selected to provide a constant pressure system and to allow for the direct measurement of the quantity of iodine adsorbed on the bed rather than monitor small changes in gas composition. This is also referred to as a "single pellet system."

The glass gas reaction chamber was connected to the feed gas header. The basket itself was suspended from a tripod device which rested on the pan of the electronic balance (Sartorius Instruments Model LC620P) used to measure the weight changes of the sorbent material. This configuration allowed the basket to be free floating within the reaction chamber. Thus it was possible to directly determine the weight change of the test material in a flowing system. Weight data were collected from the electronic balance via a serial connection to an adjacent personal computer.

Table 2. Summary of single-pellet tests.

Test No.	Size (in.)	Velocity (m/min)	CH ₃ I concentration (mg/m ³)		H ₂ O added	Temperature (°C)	Notes
			Planned	Actual ^a			
Initial series							
3	1/16	10	1000	1559		150	
4							Test aborted
5 ^b	1/8	10	1000	1275		150	
6	1/16	10	1000	1505		150	
7	1/8	10	1000	1523		150	
8	1/16	5	1000	1675		150	
9							Test aborted
10 ^c	1/16	10	1000	1190		200	
11	1/16	10	1500	1634		150	
12 ^c	1/16	10	500	837		150	
Supplemental tests							
13 ^c	1/16	10	1000	1367	yes	150	
14 ^c	1/16	10	250	355		150	
15 ^c	1/16	2	1000	1410		150	
16	1/16	1	1000	1124		150	
17	1/16	10	0	0		150	Air only
18	1/16	1	1000	1217	dry	150	
19	1/16	10	1500	2150		150	Short run
20	1/16	10	1500	1636		150	Short run
21 ^b	1/16	10	1000	1367		200	
22	1/8	10	1500	1367		150	
23 ^b	1/16	10	1000	1000	yes	150	Water data missing
24 ^b	1/8	15	1000	1000		150	Data questionable
25	1/16	10	1000	1000		150	NaZ loading
26	1/16	10	1000	1059		125	

^aActual CH₃I concentrations determined by pressure drop in the gas supply cylinder vs time measurements.

^bData from runs T5, T21, T23, and T24 not used in analysis due to equipment difficulties or questions of validity or conditions.

^cData quality may be impacted by possible temperature shift at balance.

ORNL-DWG 91-4804R

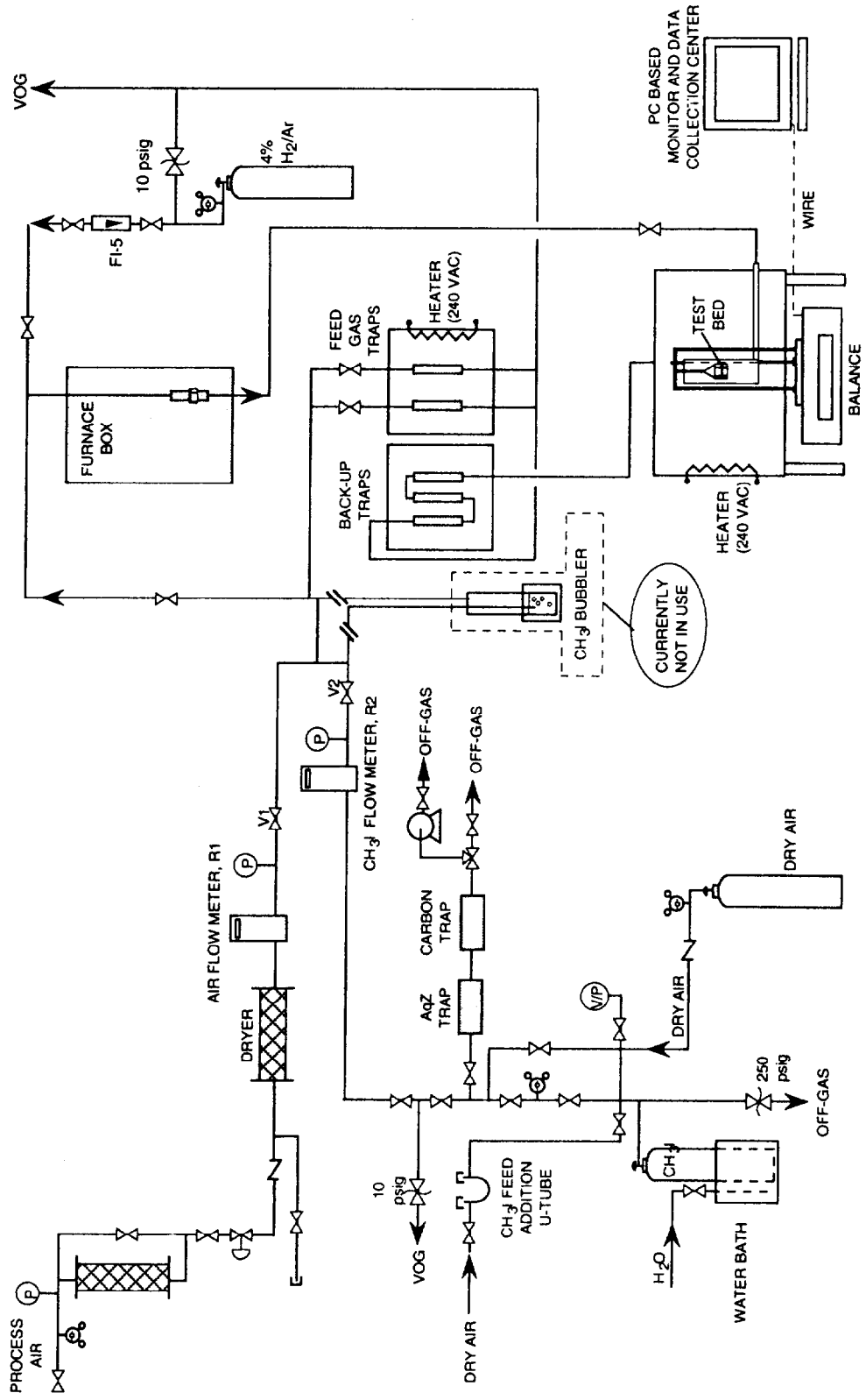


Figure 1 Schematic of experimental setup.

24th DOE/NRC NUCLEAR AIR CLEANING AND TREATMENT CONFERENCE

The glass reaction chamber was mounted in an electrically heated enclosure used to control process temperature. The heated enclosure was fabricated from a rigid insulating construction material. A secondary Plexiglas box was placed over this enclosure to prevent disturbances to the balance due to air currents in the hood. The gas that passed through the sorbent test material flowed through a series of 1-in.-I.D. backup filters loaded with either activated charcoal or silver-exchanged faujasite. The gas leaving the backup filters was discharged through the building vessel off-gas system.

The Sartorius Instruments Model LC620P poly-range electronic balance has a capacity of 120/240/620 g. Readability of the balance is 0.001/0.002/0.005 g, and standard deviation or reproducibility is $\leq \pm 0.001/0.001/0.003$ g. Gas flowrates were controlled by needle valves and standard gas regulators. Gas flowrates were monitored either by calibrated rotometers or electronic mass flow meters manufactured by Omega Engineering, Inc. The Omega flow meters have an accuracy of $\pm 2\%$ of full scale. Temperature control was accomplished by placing the entire bed in an electrically heated insulated enclosure. Temperature was controlled by a Barber-Coleman controller coupled with a type K thermocouple junction inserted directly into the flowing gas stream above the bed of adsorbent material.

Table 3 presents, in outline form, the sequence of steps used to pretreat the AgZ prior to loading with methyl iodide and the flush or post-treatment steps to flush CH_3I from the bed and thus determine the amount chemisorbed vs physisorbed. Each of these pretreatment, loading, and post-loading steps were monitored for weight changes, with the data being stored in a computer file.

Experimental Results

Optical and Supporting Characterization Studies

Five samples of the mordenite materials used in this study were analyzed for pore size distribution, density, and characterization of the uniformity of silver and iodine distribution where applicable. The samples analyzed were the 1/16-in. sodium mordenite, the 1/16- and 1/8-in. AgZ, and the 1/16- and 1/8-in. AgZ pellets from tests T19 and T20, respectively. The last two samples were analyzed only for silver and iodine distribution.

The topography of the material was shown in secondary electron images (SEI). Back-scattered electron images (BEI) showed variations in the image intensity across a portion of the pellet which is related to variations in the average atomic number in the region under examination. The specific distributions of silver, iodine, silicon, and aluminum across the specimen were shown by elemental maps.

In general, the BEI taken across the entire cross section of several fractured AgZ pellets showed no significant variation in the average atomic number (Walker, 1994). On one or two pellets, some localized accumulation of the silver was noted in a few small areas. Aside from these few areas, no silver gradient was noted within the pellets. Prior to hydrogen pretreatment, the pellets displayed uniform distribution of the silver. However, following pretreatment with 4.5% hydrogen and subsequent loading with methyl iodide (samples from tests T19 and T20), very small particles (< 1 or 2μ) were seen on the surfaces of the larger crystalline structure. An elemental map obtained through energy-dispersive X-ray analysis of one pellet showed that these fine particles contain a higher concentration of silver than the concentration in the surrounding material. In addition to the presence of these fine silver-containing particles, there remained a relatively uniform distribution of silver across the mordenite pellet cross section. No specific area of silver depletion was detected when compared with the silver distribution prior to hydrogen pretreatment and iodine loading.

24th DOE/NRC NUCLEAR AIR CLEANING AND TREATMENT CONFERENCE

A low concentration of iodine was also observed to be uniformly distributed in the mordenite pellets analyzed from Test T19 (24% final conversion) and Test T20 (35% final conversion). Examination of the fine silver-containing particles showed that while these are rich in silver, they contained virtually no iodine. Using the same technique on the larger mordenite particles or crystals showed that they, on the other hand, contained a low concentration iodine that appeared to be uniformly distributed.

Table 3 Outline procedure for single-pellet CH₃I loading tests.

Bed pretreatment (standard for all tests)
Drying
24 h air
11.4 L/min of dry instrument air
Temperature: 150°C
Nitrogen temperature equilibration
4+ h N ₂
0.4 L/min
Temperature: 200°C
Silver reduction
8 to 20 h 4% H ₂ /Ar
0.4 L/min
Temperature: 200°C
Second nitrogen temperature equilibration
4+ h N ₂
Same flow rate as that to be used in CH ₃ I loading
Same temperature as that to be used in CH ₃ I loading
Loading conditions (specific test conditions listed in Table 2)
H ₂ O vapor content (dew point)
>-15°C (7.3×10^{-5} mol/L) or -40°C (5.6×10^{-6} mol/L)
Pellet diameters
1/16 or 1/8 in.
Gas velocities
1, 2, 5, or 10 m/min
CH ₃ I gas concentrations
250, 500, 1000, or 1500 mg/m ³
Bed temperature
125, 150, or 200°C
Air flush (standard for all tests)
24+ h air
11.4 L/min or dried instrument air
Temperature: 150°C

The SEI of the pellets examined showed the voids and macropores present in this material. The SEI also showed that there was the possibility for significant variation from pellet to pellet. These variations fell into two categories. First there was some variation in the general structure of the pellets. Some were observed to have substantial voids in the pellet interior, while other pellets appeared to contain separate cores. The second type of variation involved the crystalline particles that comprised the overall structure. Some were well formed, and others had very rough and irregular surfaces. In

24th DOE/NRC NUCLEAR AIR CLEANING AND TREATMENT CONFERENCE

addition, they appeared to vary in size and overall shape. Both the 1/16- and 1/8-in. pellets were composed of individual crystals estimated to be 4.0μ in equivalent spherical diameter.

What appears to be a shrinking core behavior, as shown by color changes in the pellets, was observed through unpublished optical photographs made during the deep-bed studies previously completed and reported by this author [Jubin (1980, 1982)]. The test from which these pellets were taken was conducted under the following conditions: a bed temperature of 200°C , a CH_3I concentration of 1000 mg/m^3 , and a gas velocity of 10 m/min at standard temperature and pressure. The loadings for the individual pellets were not determined, and only the average loading on each of the 2.54-cm-thick bed segments was measured by tracer analysis. At very low CH_3I loadings on the AgZ (~3% average conversion) the pellet from the fourth or last bed segment shows no sign of any visible ring. As the average bed segment loading increases, a clearly developed ring around the core is apparent. This is shown in Fig. 2 at an average bed segment conversion of ~19%. However, at higher average loadings (~40% conversion), the color variation across the diameter of the pellet virtually disappears (Fig. 3). In Fig. 3, which shows several pellets from the first bed segment, it appears that only a very small core remains in one pellet while in the other pellet no core is visible.

Baseline Adsorption Data

Water Uptake by AgZ

One obvious concern in analyzing the CH_3I uptake data was the possible impact of concurrent weight gain by the adsorption of water from the flowing gas stream. Test T17 was performed to measure the quantity of water adsorbed as a function of time. After approximately the first 16 h that the bed was subjected to the flowing instrument air at 150°C , an observed gain of approximately 0.05 g had occurred on the 2.5416-g bed and the loading appeared to have leveled off. After 40 h the total had risen to about 0.07 g. Over the next 50 h, the loading appeared to stabilize at a total weight gain of about $0.075 \pm 0.005 \text{ g}$. These values must be compared with the total weight gains observed when CH_3I was present in the flowing gas stream to determine their significance and possible impact on the CH_3I loading data. The typical weight gain was on the order of 0.45 g in 60 h, as in the case of T10.

CH_3I Loading on NaZ

It was assumed at the start of this study that any weight gain on the mordenite pellet was primarily associated with chemical bonding with the silver contained in the pellet. Test T25 was conducted to determine the loading rate and quantity of CH_3I adsorbed on the unexchanged sodium form of the mordenite. In this run, 0.0807 g was loaded over the 22-h test period. Following the loading cycle, an air purge of 70 h was conducted. During this period, a net gain of 0.0353 g was observed that must be attributed to a water vapor. The total CH_3I loading should be compared with loading curves from tests such as T3, in which 0.335 g was gained over the same time period to examine the significance. Based on these data, it would appear relatively safe to assume that the observed weight gains on the beds that were measured during the CH_3I loading tests required a chemical reaction between the CH_3I and the silver.

CH_3I Adsorption Studies

Figures 4 and 5 are examples of the CH_3I loading curves that were obtained for all of the experimental runs. The air flush portions of the tests may also be included in the loading files as this phase of the tests was conducted as a continuation of the test conditions with only the CH_3I flow

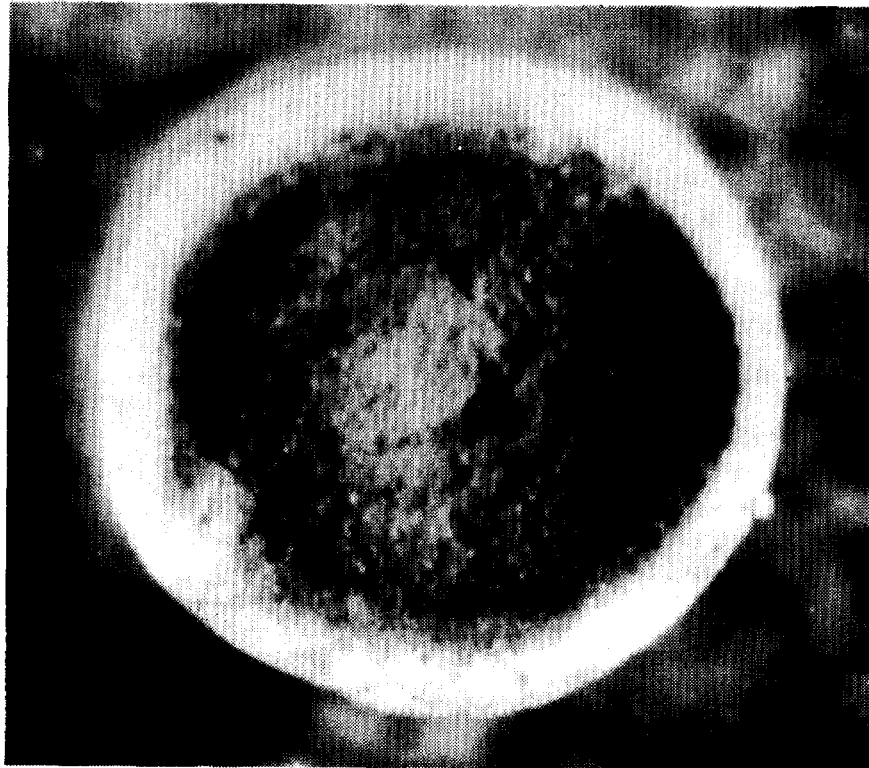


Figure 2 Optical image of 1/16-in. AgZ from bed with an average conversion of ~19%.



Figure 3 Optical image of 1/16-in AgZ from bed with an average conversion of ~40%.

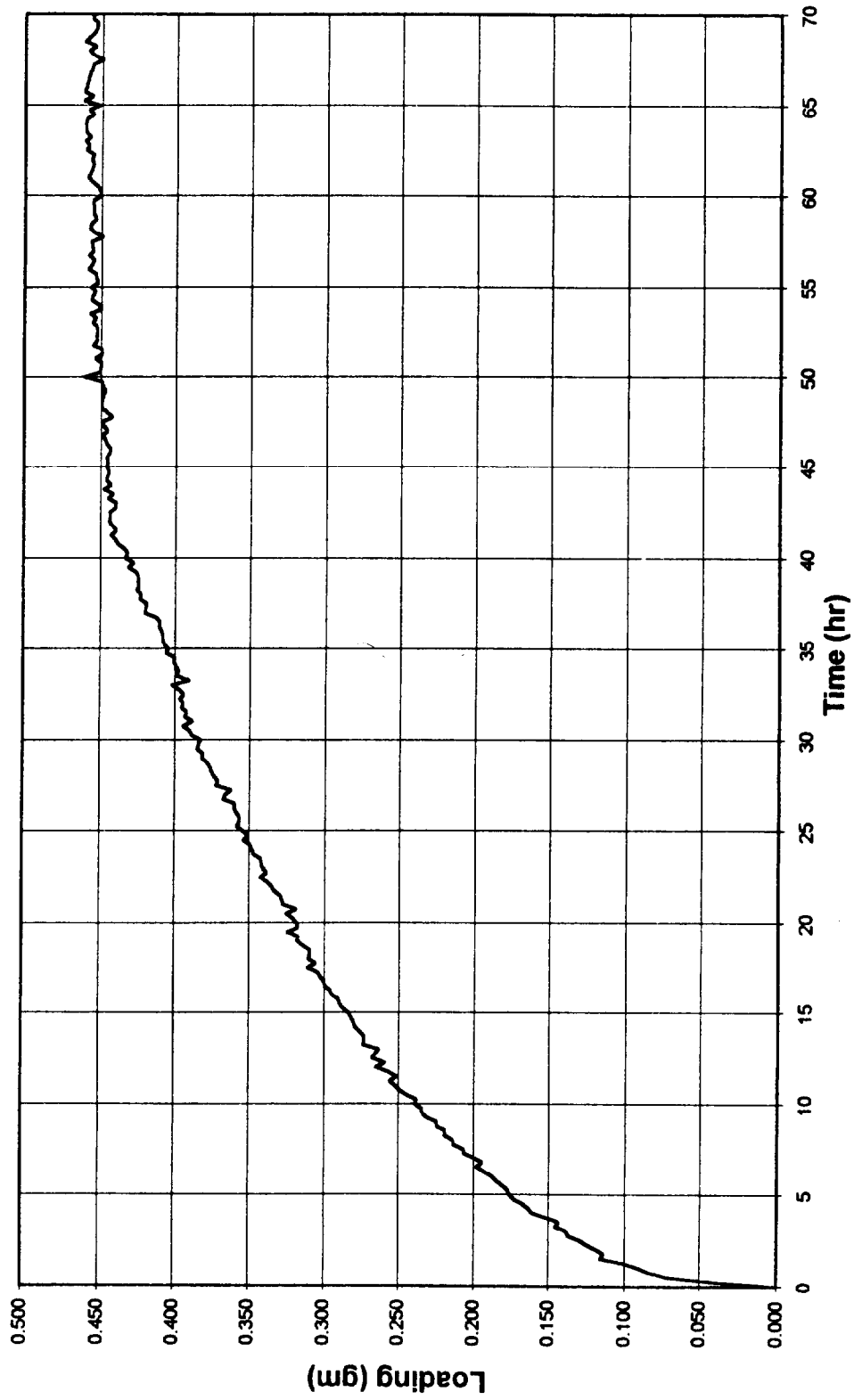


Figure 4 CH₃I loading curve from Test T3.

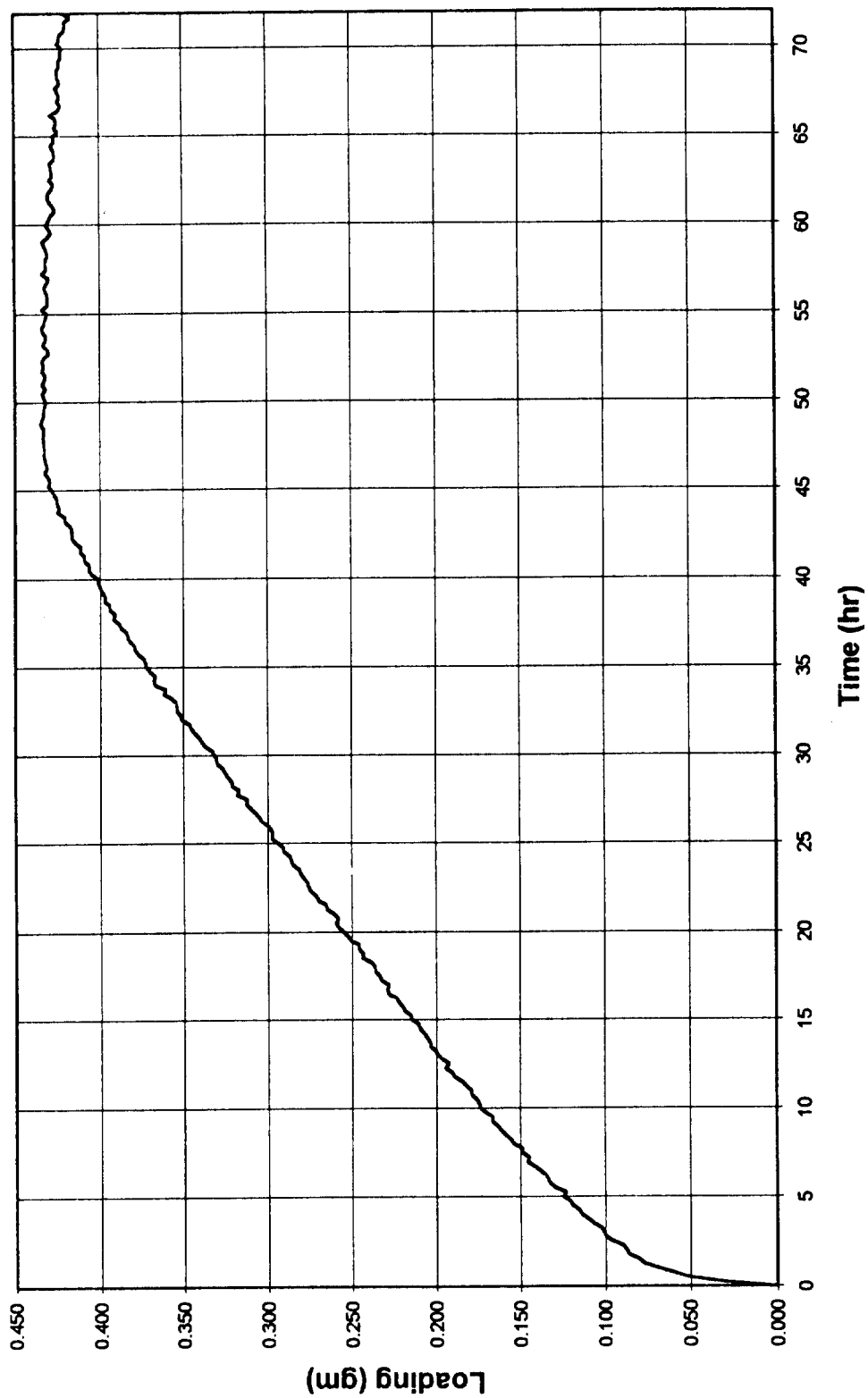


Figure 5 CH₃I loading curve from Test T22.

24th DOE/NRC NUCLEAR AIR CLEANING AND TREATMENT CONFERENCE

stopped. The total weight loss from the pellets during the air flush was generally about 1 to 2% of the total iodine loaded. A summary of the actual test conditions is presented in Table 2.

Discussion

Analysis of Optimization Techniques and FORTRAN Implementation of Potential Models

To determine the mechanism(s) controlling the mass transfer of CH_3I onto the silver-exchanged mordenite, the experimentally obtained data were compared against widely accepted models of adsorption behavior. Each of the nine models from the literature was translated into appropriate FORTRAN code using Microsoft Corporation's Powerstation FORTRAN compiler, Version 1.0. In each case, the formulation of the model equations is such that given the appropriate rate-controlling parameters, the degree of conversion or a mass flux at a specific time can be directly or indirectly computed. The term "indirectly computed" means that the conversion cannot be directly computed but must be found by iteration or by some root-finding method. The potential models were evaluated against the observed adsorption uptake curves. The best values for the rate-controlling parameters were determined by linear or multidimensional regression techniques using the experimentally obtained loading data as the reference.

The two primary criteria applied to the selection of the appropriate model for this system were (1) the ability of the model to account for the systematic variation in operating parameters without arbitrary changes in the adjustable parameters and (2) the determination of consistent diffusion coefficients for the experimental conditions evaluated.

Two classes of data fitting models were employed in this study. The first, and by far the simplest, was the single parameter model. In this case, it was a relatively simple matter to find the minimum using any of a variety of minimization techniques. The FORTRAN function FMIN described by Forsythe et al. (1977) was used for all single parameter models. This function used a combination of a golden section search technique and successive parabolic interpolation. This provided a very robust function not requiring the determination of derivatives.

Several of the models required multidimensional minimization to extract the relevant parameters. These models included both the full shrinking core and the bimodal. The determination of "best fit" to the experimental data in the case of a multiparameter model was significantly more complex. Press et al. (1992), in discussing multidimensional minimization, recommend the POWELL method as being faster in most cases and state that it can be used when derivatives are not easy to calculate.

CH_3I Adsorption-Model Comparisons

General Model Requirements

In the identification of a model to describe the adsorption of CH_3I onto silver-exchanged mordenite, it was required that certain general observations be accounted for by the selected model. These were as follows:

1. The possible formation of a rapidly shrinking shell of reacted material as observed in Figs. 2 and 3, noting, of course, that the unreacted core was no longer visible once 30-50 % conversion was achieved.

Table 4 Comparison of the simple sum of the square of the error in the conversion terms for the shrinking core models.

Run No.	Gas film		Ash diff		Rxn control		Gas film + Ash + Rxn			
	k_g (cm/s)	Error ^a	D_c (cm ² /s)	Error	k_s (cm/s)	Error	k_g (cm/s)	D_g (cm ² /s)	k_s (cm/s)	Error
T3	7.44E-02	2.46E+00	1.05E-03	6.89E-03	1.05E-01	1.16E+00	9.90E+99	1.05E-03	1.02E+06	6.89E-03
T6	7.76E-02	3.44E+00	1.33E-03	4.52E-02	1.20E-01	1.16E+00	9.90E+99	1.56E-03	8.42E-01	1.73E-02
T7	1.14E-01	1.74E-01	1.70E-03	6.41E-01	1.36E-01	1.76E-01	9.18E+99	4.72E+11	1.36E-01	1.76E-01
T8	4.20E-02	1.93E-01	3.17E-04	8.44E-01	5.00E-02	2.27E-01	9.20E+99	4.74E+11	5.00E-02	2.27E-01
T10	1.13E-01	4.56E+00	2.75E-03	4.73E-01	2.08E-01	1.85E-01	9.90E+99	8.86E-03	2.99E-01	3.13E-02
T11	8.33E-02	5.30E-01	6.85E-04	4.50E-03	1.01E-01	3.49E-01	9.90E+99	6.85E-04	1.36E+06	4.50E-03
T12	4.74E-02	2.30E-02	1.87E-04	1.91E-01	5.20E-02	1.43E-02	9.90E+99	3.01E-03	5.59E-02	1.27E-02
T13	5.52E-02	3.94E-02	4.85E-04	9.70E-01	6.76E-02	6.93E-02	9.64E+99	4.22E+12	6.76E-02	6.93E-02
T14	1.61E-01	3.17E-01	9.94E-04	8.08E-02	1.86E-01	2.03E-01	9.90E+99	1.66E-03	4.95E-01	3.26E-02
T15	4.82E-02	2.55E-02	3.32E-04	1.19E+00	5.67E-02	9.42E-02	9.89E+99	9.13E+12	5.67E-02	9.42E-02
T16	5.80E-02	4.39E-01	6.59E-04	6.81E-01	7.63E-02	6.20E-02	9.90E+99	4.12E-03	9.24E-02	1.97E-02
T18	5.08E-02	3.32E-02	3.10E-04	4.93E-01	5.87E-02	2.43E-03	9.90E+99	1.35E-02	6.03E-02	1.87E-03
T19	1.14E-01	6.12E-02	5.08E-04	1.60E-04	1.27E-01	4.93E-02	9.90E+99	5.08E-04	6.11E+06	1.60E-04
T20	2.87E-01	2.11E-01	3.88E-03	1.87E-03	3.40E-01	1.44E-01	9.90E+99	4.19E-03	5.05E+00	1.21E-03
T22	9.21E-02	1.05E+00	2.16E-03	2.98E-01	1.23E-01	3.89E-01	9.90E+99	4.38E-03	2.54E-01	9.79E-02
T26	7.36E-02	9.91E-01	5.08E-04	9.40E-02	8.67E-02	7.95E-01	9.90E+99	5.08E-04	2.07E+13	9.40E-02
Total errors		1.46E+01		6.01E+00		5.08E+00				8.87E-01

^aError terms are the resultant sum of the square of the error between the experimental data and the proposed model.

24th DOE/NRC NUCLEAR AIR CLEANING AND TREATMENT CONFERENCE

2. Fairly uniform iodine loading across the pellet diameter at 30 to 40% conversion of silver or greater.
3. Observation from past studies that higher loading was achieved prior to breakthrough with increased operation temperature.

Shrinking Core Model

The regression analyses for the shrinking core model is presented in Table 4. By examining this table, it is clear that the diffusion through the gas film was not the controlling mechanism. In virtually every case in which the parameters for three terms of the full shrinking core model were used as adjustable parameters in the minimization of the error between the model and experimental data, the computed value for k_g was on the order of 10^{100} cm/s. This value was the upper limit set in the search routines. In the few cases where it did not reach the upper bounds, the value is still above 10^{10} cm/s. The substitution of this value in the Eq. (5) for $\tau_{gasfilm}$ and the subsequent application into summation of the resistances showed that the resistance was mathematically negligible. Further, the values of k_g determined for the gas film alone were compared with the values of k_g as estimated by use of the Sherwood number and the molecular diffusivity D_{AB} . The values of k_g estimated by the Sherwood number were on the order of 3 to 9 cm/s. However, if the assumption was made that the controlling resistance was the gas film, then the values for k_g determined by the least-squares curve fitting method ranged from 0.04 to just over 0.3 cm/s. Finally, the shape of the uptake curve was not indicative of gas film resistance control.

Thus having ruled out gas-phase control and continuing with the shrinking core analysis, there appeared to be two distinct classes of behavior or types of loading curves. The first class may be described by diffusion control through the ash layer, which appeared to describe several of the cases (e.g., T3); however, in most of the runs, the loading curve appeared to have a "knee" which the shrinking core model cannot fit. These uptake curves tended to show a rapid weight gain followed by a slower rate of weight gain. This "knee" may also be an indicator that possibly two or more mechanisms were controlling the adsorption process and that there was a transition from one to the other.

If the ring observed on the pellets, as shown in the Fig. 3, was related to the loading of iodine on the pellet, then it was easily shown that at 40% utilization the radius of the unreacted core should be ~78% of the overall pellet radius. The observed radius in Fig. 3 was only ~27% of the pellet radius for the pellet that still shows a core. This 27% equates to ~93% conversion if a strict shrinking core model was correct. It should also be recalled that the BEI of the pellets from T19 and T20 showed no significant iodine gradient, which appeared to be relatively consistent with the photographic evidence at higher iodine loadings. These data tended to lead to the conclusion that while there may initially be the appearance of the shrinking core-type behavior, there was also a second slower process that accounted for the loading above some nominal level of loading associated with the shrinking core.

The effective diffusivity calculated from the data collected over the time periods of the first 40 data points (10 h) ranges from 1.84×10^{-4} to 3.91×10^{-3} cm²/s for the runs that did not exhibit any thermal upset in the balance. This effective diffusivity was also compared with that predicted by fundamental analysis of the zeolite pore structure and physical constants for the diffusing component. By comparison of the above effective diffusivities with the combined effective diffusivities for either the Knudsen diffusivity in the micropore/mesopore which are in the range of 5×10^{-5} to 5×10^{-4} cm²/s or the effective molecular diffusivity of $\sim 1.4 \times 10^{-2}$ cm²/s in the macropore range, it was observed that the value obtained by curve fitting falls between the two bounding cases. Using the shrinking core model, it was possible to find a set of parameters that seems to successfully model each individual loading curve. However, it was less obvious why some sets of data were diffusion controlled and other similar sets

appeared to be reaction controlled. This model by itself was unable to explain the apparent change in controlling mechanism. However, it provides strong evidence that

1. the mass transfer process was not controlled by the gas film resistance; and
2. there was a diffusional component, and the effective diffusivities in the first few hours of loading were in the range of 1.84×10^{-4} to 3.91×10^{-3} cm²/s for the runs in which the data showed no thermal upset in the balance during the initial period.

Macropore/Micropore Model

Mathematically, these two models are essentially the same. In the micropore diffusion case, the radius of the crystal is the dimensional term used, and in the macropore case, the pellet radius is the relevant term. In the case of the macropore model, the diffusivity term that is obtained from the curve fitting analysis is an effective diffusivity which contains an equilibrium constant. This equilibrium constant, under cases of a linear equilibrium, relates the adsorbed phase concentration q to the gas phase concentration C by

$$q = K^*C \quad (22)$$

The results of both micropore and macropore models obviously yield the same error terms (Table 5) and were virtually the same as those obtained for the ash diffusion term of the shrinking core model by itself. It can be noted that neither model provided a particularly good prediction of the overall experimental behavior. However, as noted above, for large values of time, a plot of the term $\ln(1 - X_B)$ vs time should yield a straight line with a slope of $-\pi^2 D_c / r_{i2}^2$ and an intercept of $\ln(6/\pi^2)$ at a value of time equal to zero if micropore diffusion is the controlling mechanism.

An example of such a plot is shown in Fig. 6. Table 6 is a tabulation of the resulting micropore diffusion coefficients obtained from the slopes of this type analysis of all data sets. The correlation coefficient values, R^2 , showed very high correlation for the linear regression of this data. This indicated that after the initial portion of the loading process, the effective micropore diffusivity was constant and, based on the data from this study, fairly consistent over a significant range of operating conditions. All the slopes of the uptake curve plotted as the $\ln(1 - X_B)$ vs time were obtained for values of time greater than 10 h. For all runs except for T12, T14, T16, T18, and T26, the value of D_c was between 2.19×10^{-14} and 3.34×10^{-14} cm²/s. There was no notable distinction in the values of the determined micropore diffusivity between pellet size or by the addition of supplemental water vapor or any of the variations in the pretreatment steps.

T12 and T14, which utilized low CH₃I gas concentrations, exhibited lower values of D_c , 9.32×10^{-15} and 1.13×10^{-14} cm²/s, respectively. It has also been noted that both of these runs were subject to some thermal instability in the early readings.

The value of D_c for T26 is also somewhat lower than the rest of the data sets. The calculated value is 1.06×10^{-14} cm²/s, which in this case could be attributed to the lower bed temperature used in this run since D_c in theory follows an Arrhenius-type temperature response.

T18, which was conducted with a dry air stream, exhibited the same type behavior as the other runs and had a comparable value for D_c of 1.59×10^{-14} cm²/s, which seemed to indicate that in the long time period, the adsorption rate may also be controlled by micropore diffusion.

T16 yielded values for D_c of 2.98×10^{-14} or 5.39×10^{-14} cm²/s, depending on which portion of the loading curve is being analyzed. It was noted from the run log that there was some shift in the CH₃I feed rate that may have occurred and was not detected until after the weekend. This may have occurred about the time that the shift in the slope occurred.

24th DOE/NRC NUCLEAR AIR CLEANING AND TREATMENT CONFERENCE

Table 5 Micropore and macropore model parameters for the full data sets.

Run No.	Micropore		Macropore	
	D_c (cm ² /s)	Error ^a	D_p (cm ² /s)	Error
T3	1.82E-14	1.16E-02	4.50E-09	1.16E-02
T6	2.26E-14	7.44E-02	5.57E-09	7.44E-02
T7	6.73E-15	6.68E-01	6.23E-09	6.68E-01
T8	5.66E-15	8.75E-01	1.40E-09	8.75E-01
T10	3.43E-14	6.74E-01	8.45E-09	6.74E-01
T11	1.20E-14	5.32E-03	2.97E-09	5.32E-03
T12	1.65E-15	1.95E-01	4.07E-10	1.95E-01
T13	7.18E-15	1.02E+00	1.77E-09	1.02E+00
T14	3.72E-15	8.75E-02	9.17E-10	8.75E-02
T15	4.90E-15	1.22E+00	1.21E-09	1.22E+00
T16	1.17E-14	7.49E-01	2.88E-09	7.49E-01
T18	3.81E-15	5.10E-01	9.39E-10	5.10E-01
T19	1.16E-14	1.31E-04	2.85E-09	1.31E-04
T20	1.66E-14	2.13E-03	1.54E-08	2.13E-03
T22	1.24E-14	3.47E-01	1.15E-08	3.47E-01
T26	5.80E-15	8.86E-02	1.43E-09	8.86E-02
Error sum:			6.53E+00	6.53E+00

^aError terms are the resultant sum of the square of the error between the experimental data and the proposed model.

The value for the y-intercept, however, was somewhat scattered. This was attributed to other mechanisms controlling the initial portions of the uptake curve. In all cases the y-intercept was numerically greater than the expected value of $\ln(6/\pi^2)$. One explanation for this observation was that the observed uptake on the pellets was slower in the initial time periods than would have been observed if all microspheres in the pellet had been exposed to a uniform value of CH₃I at time zero. This could occur if there were a second diffusional process to control the CH₃I concentration profile across the pellet during the early time periods.

The X-ray fluorescence data indicated a fairly uniform distribution of iodine across the cross section of the pellet. A uniform distribution would not be observed in the case of a strictly shrinking core or in a macropore diffusion-controlled situation. This observation was consistent with micropore diffusion playing a role in the overall controlling mechanism.

Bimodal Model

By examination of Eqs. (18) through (20), it can be observed that the bimodal model is defined by three specific parameters in addition to the physical measurement of the particle sizes and porosities. These parameters are the macropore diffusivity, D_p , the micropore diffusivity, D_c , and an equilibrium

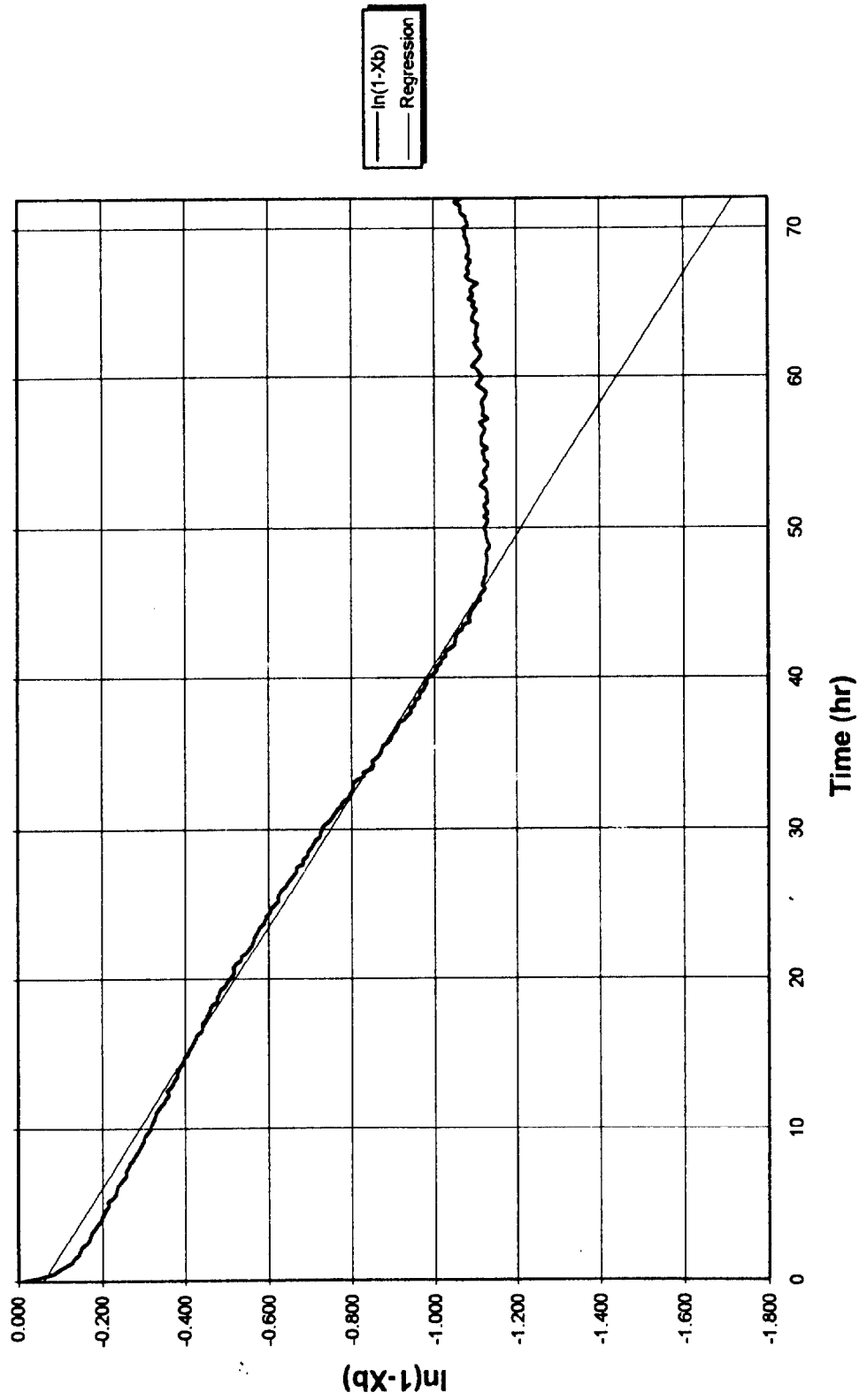


Figure 6 Determination of D_c from slope of the uptake curve plotted as $\ln(1 - X_b)$ vs time for Run T22.

Table 6: Micropore diffusivities calculated from slope of the uptake curve plotted as $\ln(1-Y_B)$ vs time.

Run No.	Range considered		Weight adjustment		Linear regression of $\ln(1-Y_B)$			Regressed D_c (cm^2/s)	
	Beginning time (h)	End time (h)	Beginning conv. (fraction)	End conv. (fraction)	Loading (g)	Slope	Intercept		Correlation coefficient (R^2)
T3	20	40	0.505	0.685		-5.98E-06	-0.275	0.99	2.42E-14
T6	10	40	0.393	0.744		-7.76E-06	-0.25	0.997	3.15E-14
T7	30	40	0.429	0.571		-8.21E-06	0.331	0.999	3.33E-14
T8	30	80	0.363	0.854		-8.23E-06	0.488	0.998	3.34E-14
T10	10	40	0.082	0.572		-7.10E-06	0.126	0.989	2.88E-14
T10	10	40	0.136	0.621	0.025	-7.73E-06	0.0953	0.991	3.13E-14
T10	10	40	0.185	0.67	0.050	-8.49E-06	0.0669	0.993	3.44E-14
T10	10	40	0.381	0.865	0.150	-1.40E-05	0.0478	0.999	5.67E-14
T11	10	24	0.313	0.475		-5.40E-06	-0.187	0.998	2.19E-14
T12	20	60	0.146	0.384		-2.30E-06	0.0906	0.998	9.32E-15
T13	20	47.25	0.214	0.566		-6.36E-06	0.226	0.997	2.58E-14
T14	10	60	0.159	0.491		-2.78E-06	-0.0698	0.999	1.13E-14
T15	30	80	0.356	0.794		-6.33E-06	0.264	0.998	2.57E-14
T16	30	70	0.525	0.896		-1.07E-05	0.53	0.976	4.34E-14
T16	30	45	0.525	0.678		-7.36E-06	0.0543	0.999	2.98E-14
T16	45	70	0.678	0.896		-1.33E-05	1.1	0.997	5.39E-14
T18	20	70	0.223	0.624		-3.93E-06	0.0409	0.999	1.59E-14
T19 ^a									
T20 ^a									
T21	45.45	60	0.635	0.772		-9.10E-06	0.454	0.99	3.69E-14
T22	10	40	0.271	0.626		-6.4E-06	-0.0585	0.995	2.57E-14
T26	10	35	0.273	0.428		-2.62E-06	-0.218	0.995	1.06E-14

^aNot determined due to short run length.

constant, q_{∞}/C_0 . These parameters can be combined along with the physical measurements into the terms α and β . Clearly, however, a difficulty in this system is that α is a function of both D_p and D_c and β is a function of α . Ideally the solution to this model would be greatly simplified if D_c , D_p , and the equilibrium constant could be determined separately.

Determination of the three parameters of the bimodal model, D_c , α , and β , by a multidimensional minimization operation was initially attempted. It was noted during the early attempts to conduct the minimization operations that as the initial search point was varied, the same values of the "optimum" parameters were not always obtained. As a result, each of the data sets was evaluated over the range of anticipated values for α and β for which the full bimodal model must be utilized.

The ranges were selected to examine the behavior of the model between the bounding conditions and thus under conditions where both mechanisms are important. Values of α and β from 10^{-3} to 10^{+2} in six even steps on a logarithmic scale were used to create a "surface map" of the errors resulting from a one-dimensional minimization of the least-squares error with the experimental data by adjusting the micropore diffusion coefficient at each node on the map grid. It was noted in these surface plots that the determination of a "best fit" to the data was not always obvious from the surface formed as a function of α and β . It was observed that there could be numerous combinations of α and β , generated by adjusting D_c , that provided nearly the same sum of the squares of the error. The minimum values for the adjustable parameters of D_c , α , and β obtained from the surface mapping approach are summarized in Table 7. However, based on the surface contours, there could be several values of the adjustable parameters that provided good fits to the experimental data. Therefore, this method provided inadequate resolution to clearly identify any "correct" or "more correct" set of parameters to describe the adsorption process of CH_3I on Ag°Z .

The tables of D_c values determined from the surface mapping approach to locating the best fit to the experimental data were then examined for similarities with the values of D_c determined from the evaluation of the slope of the uptake curve plotted as $\ln(1 - X_B)$ vs time (Table 6). The closest values to the values of D_c determined by the slope method were selected based on the lowest sum of the squares of the errors from the tables of D_c values from the least-squares curve fitting method. As can be seen from Table 7, either the same point in terms of the adjustable parameters α and β or a nearby point yielded virtually the same error term. In most cases the selected values of D_c were associated with α values of 0.001, which indicated primarily micropore diffusion. β values were generally about 10. (Note, however, that an α value of 0.001 is the smallest value evaluated in the table.)

Ma and Lee (1976) reduced the bimodal-type curve fitting problem to one of a single parameter, the micropore diffusion coefficient, D_c , through the use of calculated values for the macropore diffusion coefficient and the use of experimentally determined values for the other parameters in α and β . For the $\text{CaX}(\text{Na})$ zeolite in their study, the macropore diffusivity was estimated based on the Knudsen and molecular diffusivities. A similar analysis was conducted with the data obtained in this study. The effective macropore diffusivity for the Ag°Z was calculated to be about $0.014 \text{ cm}^2/\text{s}$, and based on the effective Knudsen diffusivity in the mesopores, the overall macropore diffusivity was estimated to be about $5 \times 10^{-4} \text{ cm}^2/\text{s}$. Finally using the value of D_c obtained from the slope of the plot of $\ln(1 - X_B)$ vs time, the effective overall macropore diffusivity along with the physical dimensions, values of α on the order of 5×10^{-6} up to about 8×10^{-5} were obtained.

The value of β appeared to be more difficult to establish. Obviously from the definition of β , it was a function of α which in turn was a function of the macropore and mesopore diffusivities. One other significant unknown remained in the β term, which was the value of the adsorption equilibrium constant. This was estimated to be about 3.4×10^5 based on the gas-phase CH_3I concentration from run T16 and the highest loading observed on the Ag°Z . The resulting value of β was about 20. β was the least well-established value, and a third optimization approach was taken to determine if a

Table 7 Bimodal model minimums based on error surface mapping.

Run No.	Best fit by mapping surface					Best fit by using closest/best match to D_c calculated by slope							
	D_f (cm ² /s)	α	β	Error ^a	$\beta/3\alpha$	D_f (cm ² /s)	α	β	Error ^a	$\beta/3\alpha$	r_a (cm)	r_i (cm)	D_c^b (cm ² /s)
T3	2.95E-14	1.000	1.000	7.81E-03	0.333333	2.95E-14	1.000	1.000	7.81E-03	0.333333	0.09808	0.0002	7.09E-09
T6	3.22E-14	0.010	1.000	1.40E-02	33.333333	3.22E-14	0.010	1.000	1.40E-02	33.333333	0.09808	0.0002	7.74E-07
T7	4.23E-14	0.001	10.000	3.40E-01	3333.333	4.23E-14	0.001	10.000	3.40E-01	3333.333	0.19715	0.0002	4.11E-05
T8	3.59E-14	0.001	10.000	4.67E-01	3333.333	3.59E-14	0.001	10.000	4.67E-01	3333.333	0.09808	0.0002	8.63E-06
T10	1.49E-13	0.001	10.000	2.96E-01	3333.333	4.64E-14	0.001	1.000	3.54E-01	333.3333	0.09808	0.0002	1.12E-05
T11	2.00E-14	1.000	1.000	4.11E-03	0.333333	2.00E-14	1.000	1.000	4.11E-03	0.333333	0.09808	0.0002	4.81E-09
T12	1.45E-14	0.001	10.000	5.51E-02	3333.333	1.45E-14	0.001	10.000	5.51E-02	3333.333	0.09808	0.0002	3.49E-06
T13	4.23E-14	0.001	10.000	4.81E-01	3333.333	1.23E-14	0.001	1.000	4.81E-01	333.3333	0.09808	0.0002	2.96E-06
T14	2.60E-14	0.100	10.000	1.98E-02	33.33333	2.60E-14	0.001	10.000	2.21E-02	3333.333	0.09808	0.0002	6.25E-06
T15	3.24E-14	0.001	10.000	5.84E-01	3333.333	3.26E-14	0.001	10.000	5.84E-01	3333.333	0.09808	0.0002	7.84E-06
T16	6.27E-14	0.001	10.000	2.02E-01	3333.333	6.27E-14	0.001	10.000	2.02E-01	3333.333	0.09808	0.0002	1.51E-05
T18	2.70E-14	0.001	10.000	1.58E-01	3333.333	2.70E-14	0.001	10.000	1.58E-01	3333.333	0.09808	0.0002	6.49E-06
T19	1.95E-14	1.000	1.000	2.32E-04	0.333333	1.95E-14	1.000	1.000	2.32E-04	0.333333	0.09808	0.0002	4.69E-09
T20	2.18E-14	0.100	1.000	1.71E-03	3.333333	2.18E-14	0.100	1.000	1.71E-03	3.333333	0.19715	0.0002	2.12E-07
T22	6.50E-14	0.001	10.000	8.72E-02	3333.333	1.95E-14	0.001	1.000	1.31E-01	333.3333	0.19715	0.0002	1.89E-05
T26	6.50E-14	0.001	10.000	8.72E-02	3333.333	1.95E-14	0.001	1.000	1.31E-01	333.3333	0.09808	0.0002	4.69E-06
Error sum: 2.81E+00											2.95E+00		

^aError terms are the resultant sum of the square of the error between the experimental data and the proposed model.
^bCalculated from a by Eq. (19).

correlation existed between the observed behavior in the early time periods and the value of β with the operational or pretreatment conditions. Table 8 is a summary of the bimodal model parameters that were obtained through a one-dimensional least-squares optimization holding D_c to the values established by the slopes of the uptake curve plotted as $\ln(1 - X_B)$ vs time and α as calculated using D_c , the calculated effective macropore/mesopore diffusivity, D_p , the measured pellet diameter, and particle diameter determined from the electron microscope images as noted above. This in essence moved all of the unknowns and variabilities to the equilibrium term contained in the β expression.

Table 8 Optimized fit using bimodal model and fixed parameters of D_c based on the slope from the plot of $\ln(1 - X_B)$ vs time in the micropore model value and α based on theoretical computed values

	D_c (cm ² /s)	α	β	Error ^a
T3	2.42E-14	1.28E-05	5.52E-01	4.72E-02
T6	3.15E-14	1.67E-05	8.10E-01	1.77E-02
T7	3.33E-14	7.67E-05	6.80E+00	3.34E-01
T8	3.34E-14	1.77E-05	8.94E+00	4.64E-01
T10	5.67E-14	2.83E-05	1.88E+00	2.56E-01
T11	2.19E-14	1.16E-05	1.02E+00	3.88E-02
T12	9.32E-15	4.94E-06	4.96E+00	5.51E-02
T13	2.58E-14	1.37E-05	4.43E+00	4.70E-01
T14	1.13E-14	5.99E-06	2.46E+00	2.23E-02
T15	2.57E-14	1.36E-05	6.80E+00	5.74E-01
T16	2.98E-14	1.58E-05	2.92E+00	2.02E-01
T18	1.59E-14	8.43E-06	4.24E+00	1.58E-01
T19 ^b	2.42E-14	1.28E-05	8.26E-01	6.65E-03
T20 ^b	2.42E-14	5.57E-05	4.08E-01	6.41E-03
T22	2.57E-14	5.92E-05	1.98E+00	9.18E-02
T26	1.06E-14	5.81E-06	8.67E-01	2.42E-01

Total error: 2.99E+00

^aError terms are the resultant sum of the square of the error between the experimental data and the proposed model.

^bShort run D_c from Run T3 was used.

This approach produced relatively good fits to the experimental data. As can be seen by comparing the error terms contained in Table 8 with those in Table 7, the fits obtained by this method were as good as those obtained from the surface mapping approach to the locating of a global minimum. In several cases, notably T3, slightly higher errors resulted from this approach than from the approach in which multiple parameters were allowed to be adjusted, but the fit with the experimental data was still very good. The overall performance of this model using a single parameter was superior to the shrinking core model with all but one parameter fixed. There was, however, no obvious trend in the resulting values of β . These values ranged from 0.4 to about 9.

Further calculation of other parameters such as the equilibrium constant contained in the β term from the values of the parameters determined as described above was thought to be invalid for several reasons. First, when one parameter is determined from a second fitted parameter, the uncertainties tend to accumulate in the resultant value. Second, in this determination, since the value of D_c was determined from the slope of the uptake curve plotted as $\ln(1 - X_B)$ vs time and α was calculated from this value and other theoretical and measured terms, all of the uncertainties will be accumulated in the single adjustable parameter. Third, as noted from the photographs of the pellets, there can be significant variations in the structure, which in turn could impact the macropore diffusivity. Since the theoretical value of D_p was used, any variation from this value would end up being observed in the fitted value of β . It can also be shown that moderate variations in the theoretical values of D_p will not have an impact through α on the least-squares regression of the data to the proposed model (Jubin, 1995). And finally, the nature of the experiments conducted was not directed toward the determination of terms such as the equilibrium constant. Therefore, it is believed that any such secondary value would be of questionable validity.

Conclusions

This study has shown that there is a slow (micropore) diffusional process controlling the latter portion of the uptake curve. This was determined to be 2×10^{-14} cm²/sec, and that the value of the diffusivity associated with this phase of the uptake was consistent over a number of runs. Based on the value of α obtained for the bimodal model, it was also shown that the process can be considered to be occurring in two steps. The time constants for the two processes are such that the macropore diffusion was virtually complete prior to any significant micropore diffusion occurring. Thus there was a shift in time prior to the start of the micropore adsorption.

One measure of this time shift was the observed shift in the y-intercept of the line describing the uptake curve plotted as $\ln(1 - X_B)$ vs time in the long time period. If no macropore diffusional resistance was observed and all microspheres were subject to a bulk gas-phase concentration equal to the bulk gas phase at time = 0, then only the micropore diffusional rate would be observed. In this case, the y-intercept would be given by $\ln(6/\pi^2)$. However, with macropore diffusional resistance and adsorption occurring in the initial phase, there is some finite time period required before the concentration of the CH₃I becomes nonzero at any point in the pellet and even longer before it reaches the bulk equilibrium concentration. This delay shifts the start of the micropore diffusion and the associated micropore uptake. Thus for any given value of D_c obtained by the slope method, the actual conversion at a given time will be less than that predicted by micropore diffusion model alone using the derived value of D_c .

The quantity and rate at which iodine was adsorbed in the macropores is then a function of the available surface area, the nature of the macropore structure, and the quantity of available silver. Based on photographic evidence, the available surface area and the pore structure was quite variable and could not be predicted by any of the process measurements made during each of the test runs. The available silver may be related to the "nonframework" silver cations in the mordenite structure, to any silver on the surface of the mordenite crystals, and to the silver nodules that appear after the hydrogen pretreatment. This may also be quite variable and the magnitude of the variation was unknown for each run. This macropore diffusion control in the initial time period would also appear to explain the appearance of the shrinking core that vanishes by the time 20 to 30% conversion occurs. One other point on this topic is that the term macropore or bimodal, in the case of this material, is a significant simplification. The pore sizes range from 20 Å to 10 μ, with a peak in the macropore region occurring at about a pore diameter of about 1 μ. Thus a continuum of pore sizes existed.

24th DOE/NRC NUCLEAR AIR CLEANING AND TREATMENT CONFERENCE

This study has determined a consistent "micropore diffusion" rate on the order of 2×10^{-14} cm²/s. It has also been shown that the bimodal model adequately explains the observed uptake behavior and the photographic as well as X-ray evidence. It has further been shown that the adsorption process described by this model can be considered a two-step process. This information is important since it is the rate of the second step that ultimately controls the final bed loading rate if high bed loadings are desired. There are, however, several questions concerning the impact of the many process and structural variables still remaining to be answered. But even without answers to every new question raised in this study, a significantly deeper fundamental understanding of the CH₃I adsorption processes onto Ag^oZ has been achieved.

In summary, considering the potential sources for experimental variation and the model sensitivity, the values determined for the bimodal model parameters, D_c , α , and β , are very consistent and clearly appear to adequately model the uptake of CH₃I on Ag^oZ over the longer time periods. In addition, the bimodal two-step process seems to explain the appearance of a "ring" or shrinking core in the pellets at low conversion and yet a uniform iodine distribution at higher loadings.

The specific conclusions drawn from this study are as follows:

1. It was shown based on both fundamental analysis and on the results of the least-squares curve fitting that the gas film resistance to mass transfer is negligible.
2. It was also shown that the system can be considered virtually isothermal. The maximum calculated temperature difference between the pellet and the bulk fluid was 0.37°C. This is an important determination in that it simplifies the modeling of the process.
3. The micropore diffusivity at 150°C as calculated from the slope of the $\ln(1 - X_B)$ vs time curve is in the range of 1.95×10^{-14} to 3.33×10^{-14} cm²/s. The error in these values as estimated from the duplicate run at the standard conditions is about 30%.
4. The bimodal model, which includes the uptake in both the macropores and the micropores, provides the most uniform ability to model the behavior of the adsorption of CH₃I onto Ag^oZ. The model parameters indicate that the uptake is occurring in a two-step manner, with the macropore uptake being much faster than the micropore uptake. This two-step process can account for the shrinking core observed at low conversions and the relatively uniform iodine concentration observed in the pellet at moderate to high concentrations.
5. The impact of the free silver observed in the mordenite structure could not be determined.

References

Burger, L. L., and Scheele, R. D., "Iodine Fixation Studies at the Pacific Northwest Laboratory," *Management Modes for Iodine-129*, W. Hebel and G. Cottone, eds., Harwood Academic Publishers, New York (1981).

Forsythe, G. E., Malcolm, M. A., and Moler, C. B., *Computer Methods for Mathematical Computations*, Prentice Hall, Inc., Englewood Cliffs, New Jersey (1977).

Jubin, R. T., "Organic Iodine Removal from Simulated Off-Gas Streams Using Silver-Exchanged Mordenite," *Proc. 16th DOE Nuclear Air Cleaning Conference*, CONF-801038, pp. 519-531 (1980).

24th DOE/NRC NUCLEAR AIR CLEANING AND TREATMENT CONFERENCE

Jubin, R. T., "Organic Iodine Removal from Simulated Off-Gas Streams Using Partially Exchanged Silver Mordenite," *Proc. 17th DOE Nuclear Air Cleaning Conference*, CONF-820833, pp. 183-198 (1982).

Jubin, R. T., "The Mass Transfer Dynamics of Gaseous Methyl-Iodide Adsorption by Silver Exchanged Sodium Mordenite," Ph.D. Dissertation, University of Tennessee, 1994; also, ORNL-6853 (1995).

Kärger, J., and Ruthven, D. M., *Diffusion in Zeolites and Other Microporous Solids*, John Wiley & Sons, Inc., New York (1992).

Kulkarni, B. D., and Doraiswamy, L. K., "Modeling of Noncatalytic Gas-Solid Reactions," in *Handbook of Heat and Mass Transfer, Volume 2: Mass Transfer and Reactor Design*, Nicholas P. Cheremisinoff, Editor, pp. 1107-1135, Gulf Publishing Company, Houston, Texas (1986).

Lee, Lap-Keung, "The Kinetics of Sorption in a Biporous Adsorbent Particle," *AIChE Journal*, vol. 24, no. 3, pp. 531-533 (1978).

Lee, Lap-Keung, and Ruthven, D. M., "Analysis of Thermal Effects in Adsorption Rate Measurements," *J. Chem. Soc. Faraday I*, vol. 75, pp. 2406-2422 (1978).

Levenspiel, O., *Chemical Reaction Engineering, Second Edition*, John Wiley & Sons, Inc., New York (1972).

Levenspiel, O., *The Chemical Reactor Omnibook*, OSU Book Store, Inc., Corvallis, Oregon (1979).

Ma, Y. H., and Lee, T. Y., "Transient Diffusion in Solids with a Bipore Distribution," *AIChE Journal*, vol. 22, no. 1, pp. 147-152 (1976).

Press, W. H., Teukolsky, S. A., Vetterling, W. T., and Flannery, B. P., *Numerical Recipes in FORTRAN: the Art of Scientific Computing, Second Edition*, Cambridge University Press, New York (1992).

Ramachandran, P. A., and Doraiswamy, L. K., "Modeling of Noncatalytic Gas-Solid Reactions," *AIChE Journal*, vol. 28., no. 6, pp. 881-900 (1982).

Ruckenstein, E., Vaidyanathan, A. S., and Youngquist, G. R., "Sorption by Solids with Bidisperse Pore Structures," *Chemical Engineering Science*, vol. 26, pp. 1305-1318 (1971).

Ruthven, D. M., *Principles of Adsorption & Adsorption Processes*, John Wiley & Sons, Inc., New York (1984).

Scheele, R. D., Burger, L. L., and Matsuzaki, C. L., *Methyl Iodide Sorption by Reduced Silver Mordenite*, PNL-4489, Pacific Northwest Laboratory (1983).

Scheele, R. D., and Burger, L. L., *Evaluation of Silver Mordenite for Radioiodine Retention at the Purex Process Facility Modification*, PNL-6261, Pacific Northwest Laboratory (July 1987).

Thomas, T. R., Staples, B. A., Murphy, L. P., and Nichols, J. T., *Airborne Elemental Iodine Loading Capacities of Metal Exchanged Zeolites and a Method for Recycling Silver Zeolite*, Idaho National Engineering Laboratory, ICP-1119 (July 1977).

Vaidyanathan, A. S., *Theoretical and Experimental Investigation of Sorption in Bidisperse Porous Particles*, PhD Dissertation, Clarkson College of Technology (September 1971).

Walker, L. R., personal communication to R. T. Jubin (March 14, 1994).

List of Symbols

b	= stoichiometric coefficient for B
C	= concentration (g/cm^3)
D_{AB}	= molecular diffusion coefficient (cm^2/s)
D_c	= intercrystalline or micropore diffusivity (cm^2/s)
D_e	= ash layer diffusion coefficient (cm^2/s)
D_p	= pore or macropore diffusivity (cm^2/s)
D_∞	= pre-exponential factor in Arrhenius expression for D
E_d	= diffusional activation energy (cal/mol)
K^*	= Henry's law constant based on q/C (cm)
k_g	= gas film mass transfer coefficient (cm/s)
k_s	= reaction rate constant for the gas solid reaction (cm/s)
m_t	= mass adsorbed at time t
m_∞	= mass adsorbed at time $t \rightarrow \infty$
N	= moles
p	= root to transcendental equations
q	= adsorbed phase concentration (g/cm^3)
R	= gas constant
R^2	= coefficient of determination
r_a	= pellet radius (cm)
r_c	= pellet core radius (cm)
r_i	= particle radius (cm)
S	= surface area (m^2/g) or (m^2/cm^3)
T	= temperature ($^\circ\text{C}$ or K)
t	= time (s)
X	= conversion

Greek Symbols:

α	= ratio of diffusional time constants $(D_c/r_i^2)/(D_p/r_a^2)$
β	= parameter defined by Eq. (20)
ε_p	= porosity of pellet
τ	= tortuosity factor
ρ_B	= molar density of B (gmol/cm^3)

Subscripts:

A	= component A (generally CH_3I)
B	= component B (generally silver, but in the D_{AB} term is air)
ex	= external
g	= bulk gas phase
0	= initial
s	= surface

Superscripts:

$^\circ$	= metallic form of silver
----------	---------------------------

Other Symbols and Notations:

$-$	= average value
-----	-----------------

DISCUSSION

BARLOW: What capacity do you believe you can be getting with your beds? From the knowledge you have now gained from your modeling, how much do you believe you could increase life? What is the typical utilization of the silver zeolite and does the information presented allow an estimate to be made of the maximum possible incorporation that might be achieved by an understanding of the controlling mechanisms?

JUBIN: In experimental tests with silver exchanged mordenite, loadings in the highest loaded segment of the bed have ranged from ~30% to ~60%, depending in large part on the operating conditions and bed depth. As can be observed from the thin bed loadings, completed as part of this test, silver utilizations of greater than 90% were achieved in numerous cases. The maximum loading that would be achieved in actual practice would be controlled by the bed design and by the operating conditions. By gaining an understanding of the controlling mechanisms through studies such as this one, the equipment and process conditions can be tailored to these mechanisms to achieve the highest practical utilization of the sorbent.